Journal of Applied Mechanics and Technical Physics, Vol. 47, No. 5, pp. 617–627, 2006

EXPERIMENTAL STUDY AND DIRECT NUMERICAL SIMULATION OF THE EVOLUTION OF DISTURBANCES IN A VISCOUS SHOCK LAYER ON A FLAT PLATE

A. N. Kudryavtsev, S. G. Mironov, T. V. Poplavskaya, and I. S. Tsyryul'nikov

UDC 532.526

The evolution of disturbances in a hypersonic viscous shock layer on a flat plate excited by slow-mode acoustic waves is considered numerically and experimentally. The parameters measured in the experiments performed with a free-stream Mach number $\mathrm{M}_\infty = 21$ *and Reynolds number* $\mathrm{Re}_L = 1.44 \cdot 10^5$ *are the transverse profiles of the mean density and Mach number, the spectra of density fluctuations, and growth rates of natural disturbances. Direct numerical simulation of propagation of disturbances is performed by solving the Navier–Stokes equations with a high-order shock-capturing scheme. The numerical and experimental data characterizing the mean flow field, intensity of density fluctuations, and their growth rates are found to be in good agreement. Possible mechanisms of disturbance generation and evolution in the shock layer at hypersonic velocities are discussed.*

Key words: *Navier–Stokes equations, hypersonic shock layer, acoustic disturbances.*

Introduction. In high-velocity high-altitude flight, the entire space between the surface of the flying vehicle and the bow shock wave (SW) even at a large distance from the leading edges is the viscous flow zone where the so-called viscous shock layer is formed. Like the boundary layer, the laminar shock layer is unstable, and perturbations developed in this layer induce a transition to a turbulent flow regime. The evolution of perturbations in the viscous shock layer and in supersonic flows with lower Mach numbers, however, may be caused by different mechanisms. The presence of numerous instability modes plays an important role in the development of instability at hypersonic velocities. Factors that can also affect the character of instability evolution are the interaction of instability waves and the SW [1], substantial deviations from a parallel flow, and velocity slip and temperature jump on the wall. In addition, one should take into account that instability waves can be excited not only by the conventional mechanism of receptivity but also by means of direct amplification of free-stream perturbations in the SW [2]. Finally, of great importance in flight conditions at high stagnation temperatures of the flow are real gas effects capable of changing the stability characteristics to a large extent.

Because of the above-listed factors, a sufficiently large amount of experimental measurements, results of the linear analysis of hydrodynamic stability (see [3, 4]), and data of direct numerical simulations [5, 6], which were accumulated during long-time research of the laminar–turbulent transition of the boundary layer at moderate hypersonic Mach numbers ($\mathrm{M}_\infty = 5$–8), cannot be extrapolated to the case of a viscous shock layer at extremely high Mach numbers ($\mathrm{M}_\infty = 15$–25). Meanwhile, the knowledge of mechanisms controlling the evolution of disturbances in a viscous shock layer is necessary to develop efficient methods of predicting and controlling the laminar–turbulent transition in hypersonic flows. This will allow a significant reduction of the drag force and heat loads and offer engineering background for production of efficient hypersonic flying vehicles.

Khristianovich Institute of Theoretical and Applied Mechanics, Siberian Division, Russian Academy of Sciences, Novosibirsk 630090; alex@itam.nsc.ru; mironov@itam.nsc.ru; popla@itam.nsc.ru; tsivan@ngs.ru. Translated from Prikladnaya Mekhanika i Tekhnicheskaya Fizika, Vol. 47, No. 5, pp. 3–15, September–October, 2006. Original article submitted October 27, 2005; revision submitted November 20, 2005.

There are some scarce experimental measurements of characteristics of fluctuations in the boundary layer at high Mach numbers [7–9]; as these data are scattered and limited, however, it is difficult to compare them with the results of the linear stability theory and with numerical simulations. In particular, these papers do not give information about the wave characteristics of disturbances and their growth rates. Some studies of boundary-layer stability on a flat plate and on a wedge were performed within the framework of an asymptotic approach for high Mach and Reynolds numbers [10, 11]. These flow regimes, however, are significantly different from flow conditions in a viscous shock layer. Receptivity and development of disturbances in a hypersonic boundary layer with $M_\infty = 15$ have been recently examined by means of direct numerical simulation [12, 13], but high Reynolds numbers prevented the formation of a viscous shock layer; hence, a developed boundary layer was actually modeled.

The present paper describes the results of numerical and experimental investigations of a hypersonic flow ($M_\infty = 21$) past a flat plate at zero incidence with a viscous shock layer formed over the entire flat-plate length. The mean flow and fluctuating characteristics were computed by means of direct numerical simulation, and the specific features of origination and evolution of disturbances in a viscous shock layer were examined by comparing the numerical data with the results of experimental measurements.

In the experiments performed, instability waves were excited by natural disturbances present in the wind-tunnel test section. The main source of disturbances was an unstable boundary layer on the nozzle walls. As was shown in [14], a supersonic boundary layer mainly emits slow acoustic waves. In a hypersonic flow in the wind-tunnel test section, one should expect weakly inclined waves to prevail, because the scatter in terms of propagation directions is limited here by a small angle of the Mach cone. Based on this fact, we confined our numerical simulations to an analysis of a two-dimensional problem of interaction of a viscous shock layer with slow-mode acoustic waves propagating at a zero angle to the incoming flow.

Experimental Conditions, Equipment, and Methods of Measurement. The experiments were performed in a hypersonic nitrogen wind tunnel of the Khristianovich Institute of Theoretical and Applied Mechanics (ITAM), Siberian Division, Russian Academy of Sciences. The model was a tapered flat plate of length $L^* = 240$ mm and thickness of 8 mm with a sharp leading edge (rounding radius of 0.1 mm). The flat-plate width was 100 mm at the leading edge and 80 mm at the trailing edge. The wedge angle of the leading edge was 7°. The side edges of the flat plate were tapered at an angle of 20°. The flat plate was mounted at zero incidence. The surface temperature changed only weakly during the experiment and was approximately equal to 300 K.

The experiments were performed for the following flow parameters: Mach number $M_\infty = 21$, Reynolds number per 1 meter $\mathrm{Re}_{1\infty} = 6 \cdot 10^5$ m^{-1}, and stagnation temperature $T_0^* = 1200$ K. The temperature factor of the model surface was $T_w^*/T_0^* = 0.25$. Owing to flow expansion in the test chamber, the free-stream Mach number at the end of the plate was higher by unity.

The pressure distributions behind the normal shock were measured at several points along the plate centerline (x coordinate) by a Pitot tube normal to the surface (y coordinate) to obtain the Mach number profiles in the shock layer. The size of the Pitot tube orifice was 0.5 mm. The pressure was registered by a TDM4-IV1 differential piezo-manometer whose readings were calibrated by a U-shaped water manometer. The effect of rarefaction and viscosity of the flow on results measured by the Pitot tube were estimated on the basis of data given in [15]. For the current test conditions, the measurement error was less than 5% in the entire flow except for the layer near the model surface, the thickness of this layer being approximately 20% of the shock-layer thickness.

To determine the Mach number profiles, one also has to know the static pressure distribution across the shock layer. The free-stream static pressure was determined from stagnation parameters. The SW slope as a function of the streamwise coordinate was found from the measured SW positions. The static pressure behind the SW was computed from the relations on the shock adiabat behind the bow shock wave with allowance for the angle between the SW and the flow and from the static pressure in the incoming flow. As the static pressure is not constant across the viscous shock layer, the value proportional to the pressure obtained in mean-flow computations was used.

The mean density and the amplitude of natural (uncontrolled) density fluctuations were measured normal to the plate surface along its centerline by the method of electron-beam fluorescence [16]. The flow was probed by an electron beam (electron energy 14 keV, current power in the beam 0.5 mA, and beam diameter 1 mm in the absence of the flow in the wind-tunnel test section). The procedure of reconstruction of the mean density and the field of density fluctuations from the fluorescence signal was described in [16]. The fluctuations were measured in a frequency range from 1 to 50 kHz. To reduce statistical noise, the distributions of density fluctuations in the

shock layer and the growth rates of disturbances were averaged in octave ranges of frequencies with the center at the frequencies $f^* = 2.8$, 4.8, 9.6, 19.2, and 38.4 kHz. The growth rates of density fluctuations in the shock layer α_i were computed along the line of the maximum disturbances measured in each frequency range by the relation $\alpha_i = -0.5d[\ln(\rho'/\rho_\infty)]/dR$. Here ρ' and ρ_∞ are the density fluctuations in the shock layer and the mean free-stream density, respectively, and $R = \sqrt{\mathrm{Re}_{x\infty}}$, where $\mathrm{Re}_{x\infty} = \rho^*_\infty U^*_\infty x^*/\mu^*_\infty$ is the local Reynolds number based on the free-stream parameters and the distance from the leading edge of the plate. The line of the maximum density fluctuations is normally located near the SW. As is shown below, the reason is SW oscillations under the action of free-stream perturbations.

Numerical Method. In the present work, we modeled the evolution of two-dimensional disturbances, which seem to be the most unstable ones at high Mach numbers ensured in the present experiments. The Navier–Stokes equations written in the form of a system of conservation laws were solved:

$$\frac{\partial Q}{\partial t} + \frac{\partial F}{\partial x} + \frac{\partial G}{\partial y} = \frac{\mathrm{M}_\infty}{\mathrm{Re}_\infty}\Big(\frac{\partial F^v}{\partial x} + \frac{\partial G^v}{\partial y}\Big). \tag{1}$$

In these equations, the vectors of conservative variables Q, inviscid fluxes F and G, and viscous fluxes F^v and G^v are

$$Q = \begin{pmatrix} \rho \\ \rho u \\ \rho v \\ e \end{pmatrix}, \qquad F = \begin{pmatrix} \rho u \\ \rho u^2 + p \\ \rho uv \\ (e+p)u \end{pmatrix}, \qquad G = \begin{pmatrix} \rho v \\ \rho uv \\ \rho v^2 + p \\ (e+p)v \end{pmatrix},$$

$$F^v = \begin{pmatrix} 0 \\ \tau_{xx} \\ \tau_{xy} \\ u\tau_{xx} + v\tau_{xy} + \varkappa \dfrac{\partial T}{\partial x} \end{pmatrix}, \qquad G^v = \begin{pmatrix} 0 \\ \tau_{xy} \\ \tau_{yy} \\ u\tau_{xy} + v\tau_{yy} + \varkappa \dfrac{\partial T}{\partial y} \end{pmatrix}, \tag{2}$$

$$\tau_{xx} = \mu\Big(\frac{4}{3}\frac{\partial u}{\partial x} - \frac{2}{3}\frac{\partial v}{\partial y}\Big), \qquad \tau_{xy} = \mu\Big(\frac{\partial u}{\partial y} + \frac{\partial v}{\partial x}\Big), \qquad \tau_{yy} = \mu\Big(\frac{4}{3}\frac{\partial v}{\partial y} - \frac{2}{3}\frac{\partial u}{\partial x}\Big).$$

The system is closed by the equation of state for a perfect gas

$$p = \rho T/\gamma. \tag{3}$$

In Eqs. (1)–(3), u and v are the x and y components of the velocity vector, respectively, p is the pressure, ρ is the density, T is the temperature, $e = p/(\gamma - 1) + \rho(u^2 + v^2)/2$ is the total energy per unit volume, γ is the ratio of specific heats, μ is the dynamic viscosity [viscosity as a function of temperature was approximated by the Sutherland formula $\mu = T^{1.5}(1 + C/T^*_\infty)/(T + C/T^*_\infty)$; for nitrogen, $C = 106.67$ K], $\varkappa = \mu/[(\gamma - 1)\mathrm{Pr}\,]$ is the thermal conductivity, $\mathrm{Re}_L = \rho^*_\infty U^*_\infty L^*/\mu^*_\infty$ is the Reynolds number based on the free-stream parameters (marked by the subscript "∞") and flat-plate length L^*, M_∞ and U_∞ are the free-stream Mach number and velocity, and Pr is the Prandtl number; dimensional quantities are marked by the asterisk. In the present work, we had $\mathrm{Re}_L = 1.44 \cdot 10^5$.

In writing the equations in dimensionless form, the density, temperature, and viscosity were normalized to their free-stream values; other scale factors were the velocity of sound c^*_∞ for velocity components, $\rho^*_\infty c^{*2}_\infty$ for pressure, and the plate length L^* for geometric dimensions.

The algorithm used for direct numerical simulation of the evolution of disturbances in a hypersonic shock layer should satisfy two conditions: 1) ensure a reliable (without numerical oscillations) shock-capturing computation of strong shock waves; 2) possess high accuracy in modeling the propagation of wave disturbances. The total variation diminishing (TVD) schemes widely used in computational aerodynamics do not completely satisfy the second requirement, because the accuracy of their approximation decreases to the first order at each smooth extreme point of the solution. As a consequence, high numerical viscosity is introduced into the solution, which can lead to nonphysical decay of perturbations.

Convective fluxes in the present work are computed by an MP5 (monotonicity-preserving, 5th order) scheme developed in [17]. The fluxes through the faces between the cells are computed by piecewise-polynomial reconstruction of the 4th order; as a result, the scheme has the 5th order of approximation on smooth solutions. In the

neighborhood of discontinuities, the reconstructed fluxes are bounded for the solution to preserve monotonicity; the scheme has a built-in analyzer, which can distinguish between solution discontinuities and smooth extreme points. The fluxes are reconstructed in local characteristic variables; prior to reconstruction, the characteristic fluxes are split into positive and negative parts, which is done in the present work by the so-called global Lax–Friedrichs splitting.

Diffuse terms in system (1) are approximated by the 4th order finite differences on a template containing 5×5 cells [18]. Integration in time is performed by the 3rd order explicit Runge–Kutta scheme (RK TVD-3) preserving monotonicity of the solution.

The computational domain is a rectangle with a certain part of the lower side coinciding with the plate surface. The left (input) boundary is located at a distance of several computational cells upstream from the leading edge of the plate. The height of the computational domain is chosen such that the bow SW emanating from the leading edge does not interact with the upper boundary. The right (output) boundary is moved downstream from the trailing edge of the plate to the cross section $x = 1.042$ for the flow in the exit cross section to be completely supersonic.

A steady flow was computed first with a uniform hypersonic flow directed along the x axis being set on the left and upper boundaries. On the right boundary, the solution was extrapolated from inside the computational domain. As the rarefaction effects in the problem considered are fairly significant (the streamwise velocity u on the plate surface is smaller than the free-stream velocity by an order of magnitude), the boundary conditions on the flat plate take into account the velocity slip and temperature jump:

$$u = \frac{2 - a_u \alpha_u}{\alpha_u} \lambda \frac{\partial u}{\partial y}, \qquad T - T_w = \frac{2 - a_e \alpha_e}{2\alpha_e} \frac{\gamma}{\gamma - 1} \frac{\lambda}{\mathrm{Pr}} \frac{\partial T}{\partial y} \quad \text{for} \quad y = 0,\ 0 < x < L. \tag{4}$$

Here $\lambda = \sqrt{\pi/2}\,\mu/\sqrt{p\rho}$ is the mean free path of the molecules, α_u and α_e are the momentum and energy accommodation coefficients, which are assumed to be equal to unity, and $a_u = 0.858$ and $a_e = 0.827$ are the coefficients whose values were obtained from an approximate solution of the Boltzmann equation in the Knudsen layer [19]. The slip conditions (4) were used previously, in particular, in numerical simulation of a hypersonic flow around a hollow cylinder–flare configuration; the results obtained are in good agreement with DSMC data. The boundary conditions on the flat plate were supplemented by the no-slip condition $v = 0$ for the vertical component of velocity and by the condition $\partial p/\partial y = 0$ for pressure. Symmetry conditions were set on the remaining part of the lower boundary.

Dummy cells located outside the computational domain were used in the numerical implementation of the boundary conditions.

The computational grid was uniform and consisted of 1050×240 cells. The computational code was parallelized with the use of an MPI library to perform computations on multiprocessor computers, which involved up to 10 processors of the Siberian Supercomputer Center.

The computed mean flow was compared with available experimental data. Figure 1a–c shows the computed (solid curves) and experimental (points) profiles of the mean density in cross sections $x = 0.229$, 0.313, and 0.646. The computed and experimental distributions of the Mach number in the same cross sections are plotted in Fig. 1d–f. It is seen from Fig. 1 that the overall agreement of computed and measured results is fairly good. Some difference in the mean density is caused by significant expansion of the probing electron beam owing to electron–molecule collisions in high-density regions and by smoothing of the real density profile. As a whole, the numerical algorithm offers an adequate description of the mean flow in the shock layer.

When the steady solution of the problem of the flow past a flat plate was found, the problem of interaction of the shock layer with external disturbances was solved. The variables on the left boundary were defined as a superposition of the steady main flow and a planar monochromatic acoustic wave of the slow mode:

$$\begin{pmatrix} u' \\ v' \\ p' \\ \rho' \end{pmatrix} = A \begin{pmatrix} -\cos\theta \\ \sin\theta \\ 1 \\ 1 \end{pmatrix} \exp\left[i(k_x x + k_y y - \omega t)\right].$$

Here θ and A are the angle of incidence of the acoustic wave (in the present work, $\theta = 0$) and the wave amplitude; $k_x = k\cos\theta$ and $k_y = -k\sin\theta$ are the components of the wave vector related to the dimensionless frequency

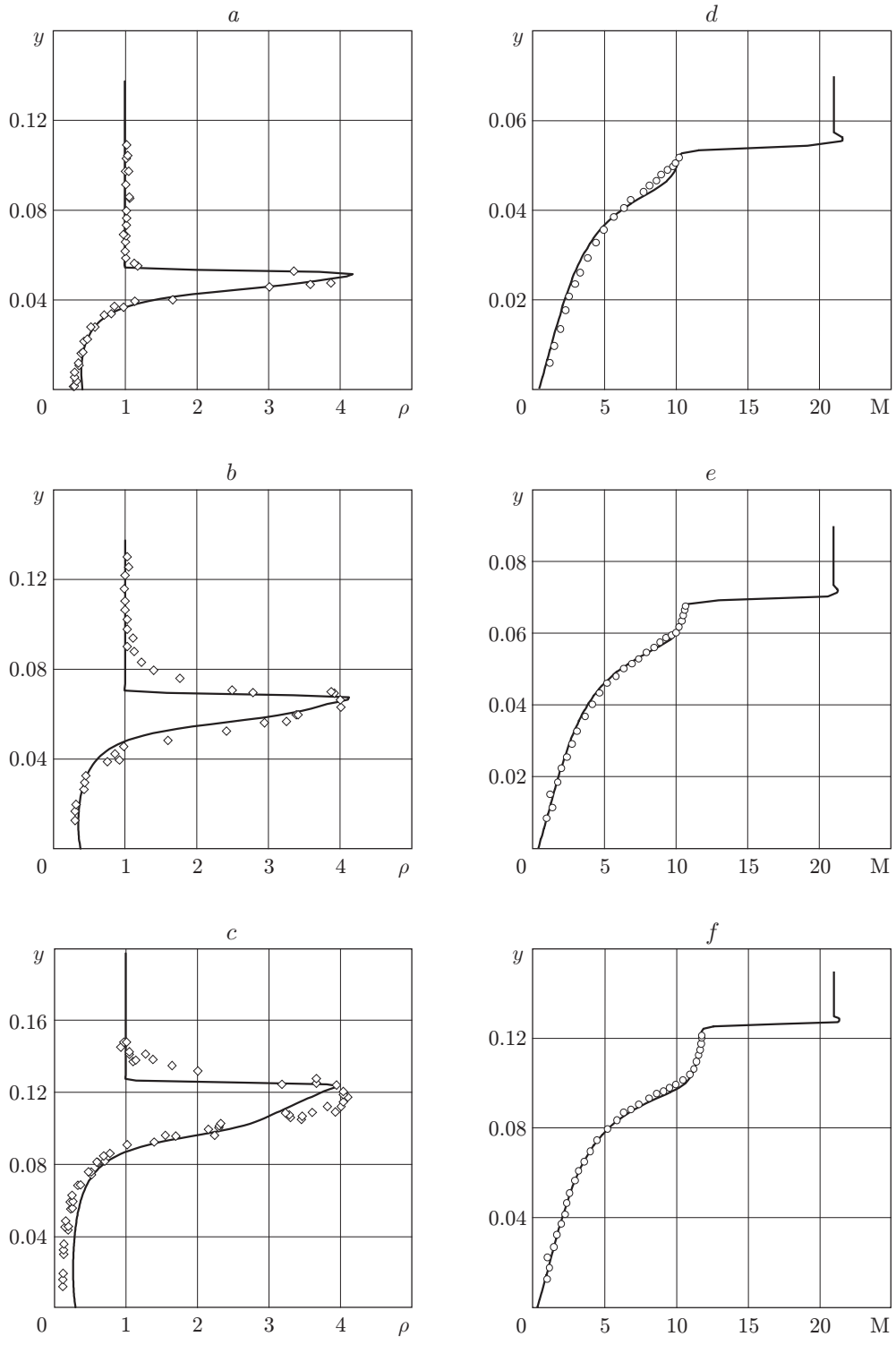

Fig. 1. Computed (solid curves) and experimental (points) profiles of the mean density (a–c) and distributions of the Mach number (d–f) in different cross sections: $x = 0.229$ (a and d), 0.313 (b and e), and 0.646 (c and f).

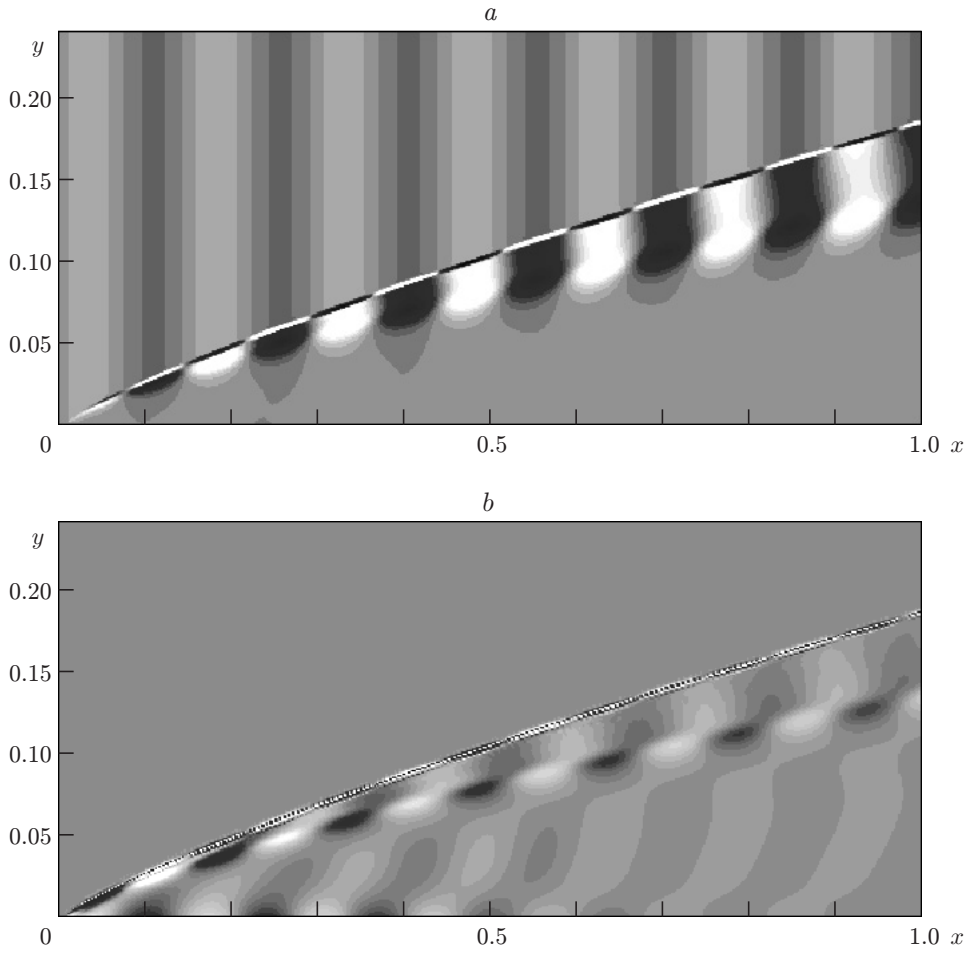

Fig. 2. Isolines of the amplitudes of density fluctuations in the shock layer (a) and fields of vorticity fluctuations (b) for $f^* = 38.4$ kHz.

$\omega = 2\pi f^* L^*/c^*_\infty$ by the dispersion relation $k = \omega/(\mathrm{M}_\infty \cos\theta - 1)$. Temperature perturbations on the plate surface were assumed to be zero ($T'|_{y=0} = 0$) by virtue of the significant thermal inertia of the flat plate; thus, the wall temperature was equal to the plate temperature obtained previously in solving the steady problem. When the acoustic disturbances were introduced, the Navier–Stokes equations were integrated up to the moment the unsteady solution reached a steady periodic regime.

Computations with the amplitudes of external acoustic disturbances $A = 0.0028$–0.0400 were performed ($A = 0.0400$ corresponds to the maximum value of dimensionless spectrum-integrated density fluctuations measured in the free stream). Within the amplitude range used, the amplitude of disturbances generated in the shock layer turned out to be linearly dependent on A. The data computed for $A = 0.028$ are given below.

Comparison of Experimental and Numerical Data. The field of density fluctuations in the shock layer up to a certain time is plotted in Fig. 2a for the frequency $f^* = 38.4$ kHz (corresponding to the dimensionless frequency $\omega = 810.25$). The light and dark regions indicate the decrease and increase in density, respectively. The most intense perturbations of density are observed on the SW and on the upper boundary of the viscous boundary layer. The maximum of fluctuations on the boundary-layer edge is several times smaller than the amplitude of density fluctuations on the SW. The changes in density in these regions are opposite in phase. For the same frequency, Fig. 2b shows the field of vorticity fluctuations in the plane (x, y). The light and dark regions refer to differently directed vectors of vorticity fluctuations. It is seen that there are counter-rotating vortices in the shock layer, which occupy the region between the SW and the boundary-layer edge. The centers of the vortices are located on the boundary between the dark and light regions (Fig. 2a).

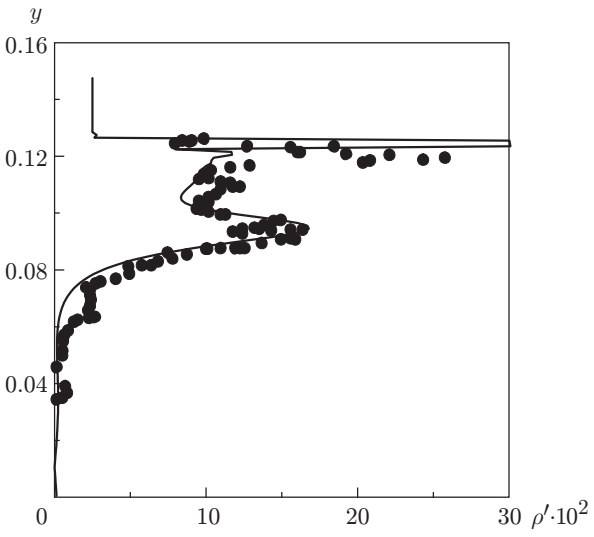

Fig. 3

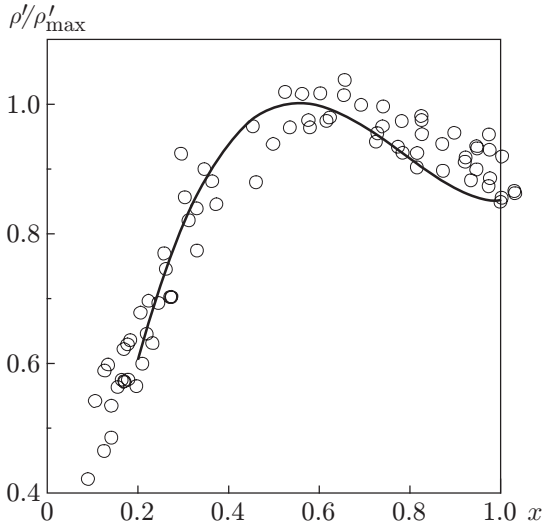

Fig. 4

Fig. 3. Fluctuations of the absolute value of density in the cross section $x = 0.63$ for $f^* = 38.4$ kHz: the solid curve shows the computed results, and the points are the experimental data.

Fig. 4. Experimental (points) and computed (solid curve) distributions of the amplitudes of density fluctuations along the flat plate for $f^* = 38.4$ kHz.

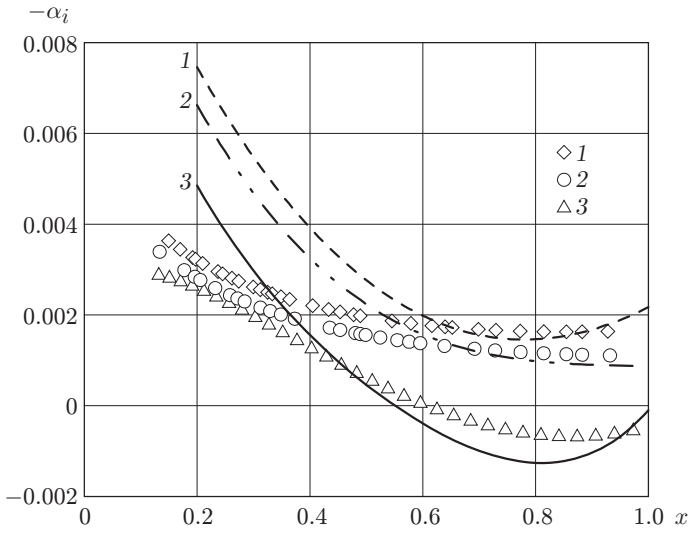

Fig. 5. Experimental (points) and computed (curves) growth rates of density fluctuations on the SW versus the streamwise coordinate: $f^* = 9.6$ (1), 19.2 (2), and 38.4 kHz (3).

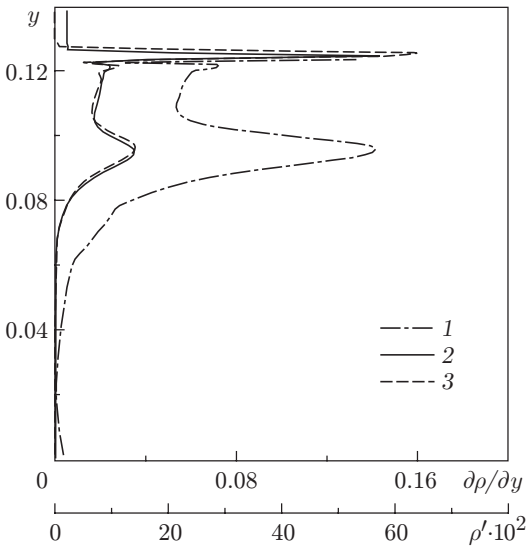

Fig. 6. Computed distributions of the mean density gradient (1), density fluctuations (2), and the distribution of model density fluctuations (3) in the cross section $x = 0.63$.

The computed distributions of density fluctuations across the shock layer are in good agreement with the experimental results. The solid curve in Fig. 3 shows the computed transverse profile of the absolute value of density fluctuations in the cross section $x = 0.63$, where two maximums are clearly displayed. The experimental data were obtained from the signal of nitrogen fluorescence with the use of deconvolution by the Fourier method for a triangular instrument function with the base width equal to the maximum diameter of the electron beam scattered by the gas (4 mm). After that, the density fluctuations were recovered by the technique proposed in [16]. Qualitatively, the computed and experimental results are in agreement, though the recovered distribution has some deconvolution artifacts in the form of additional peaks. The high statistical noise of the signal of fluctuations does not allow the use of the procedure described to obtain quantitative data on the distribution of fluctuations across the shock layer and to compute the growth rates of disturbances individually for each region of disturbance propagation.

For the central frequency of the band $f^* = 38.4$ kHz, Fig. 4 shows the experimental values of the amplitudes of density fluctuations along the plate normalized to their maximum value (points) and the computed absolute values of the maximum density fluctuations on the shock waves (solid curve). The curve was obtained by averaging the computed data for several times and in the corresponding octave frequency band with allowance for the measured distribution of intensity of density fluctuations over the frequency range. The computed and experimental data are seen to be in good agreement.

Figure 5 shows the experimental and computed growth rates of density fluctuations on the SW versus the streamwise coordinate. Points 1–3 correspond to experimental dependences of the growth rates of disturbances for the octave band with the central frequency $f^* = 9.6$, 19.2, and 38.4 kHz ($\omega = 202.6$, 405.0, and 810.25, respectively); curves 1–3 are the computed dependences for the corresponding frequencies of slow acoustic disturbances of the external flow. The computed dependences were also averaged in the octave frequency band. The computed and experimental growth rates of disturbances on the SW as functions of the x coordinate are in good agreement for $x > 0.5$.

Figure 6 shows the numerical distributions of the mean density gradient (curve 1 is plotted for the SW only because of the high gradient of the mean density on the shock wave) and density fluctuations (curve 2) in the cross section $x = 0.63$. The maximums of fluctuations are seen to coincide with the maximums of the gradient of the density distribution. This allows us to assume that the density fluctuations are caused by vortex-induced oscillations of the mean-flow field in the shock layer normal to the plate surface (see Fig. 2b) and by SW oscillations caused by the action of the incident acoustic wave. Figure 6 also shows the distribution of density fluctuations obtained

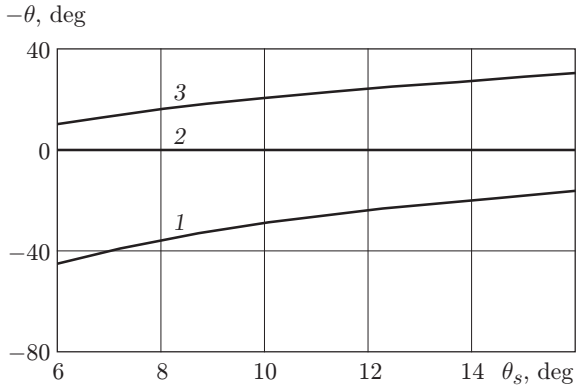

Fig. 7. Critical angles of propagation of slow acoustic waves in the free stream θ versus the angle of SW inclination to the flow centerline θ_s: curve 1 shows the critical angle of origination of fast acoustic waves behind the SW, curve 2 refers to $\theta = 0$ and curve 3 shows the critical angle of origination of slow acoustic waves behind the SW.

with small perturbations of the computed numerical mean density profile normal to the surface (curve 3). It was assumed that the amplitude of fluctuations of the normal velocity is proportional to the value of the mean normal velocity. This assumption allows determining the maximum fluctuations of velocity on the SW and zero fluctuations of velocity on the model surface. Curves 2 and 3 in Fig. 6 are in good agreement, which supports the assumption made. This model also explains the 180° phase shift between the fluctuations on the boundary-layer edge and on the SW and the large difference in their amplitude.

It should be noted that two maximums of density fluctuations with a 180° phase shift were also observed in a hypersonic wake flow [20] and in the shock layer on a compression surface [21] in the case of introduction of periodic controlled disturbances. It was also shown [20, 21] that more intense density fluctuations refer to the SW position, whereas less intense fluctuations are located on the boundary-layer edge (or on the upper boundary of the shear layer in the case of the wake flow).

It seems of interest to compare the data obtained with the known linear theory of disturbance–SW interaction [2]. According to this theory, the acoustic disturbance can pass through the SW only in the range of angles of propagation of external disturbances bounded by critical angles. Based on the measured and computed data, the SW inclination angle θ_s in the case considered varies from 16° near the leading edge of the plate to 7.5° at the end of the plate. Figure 7 shows the critical angles of propagation of slow acoustic waves in an undisturbed hypersonic flow versus the angle θ_s for $M_\infty = 21$ (curves 1 and 3). Acoustic disturbances can pass beyond the SW only if the angle of their propagation θ is below curve 1 corresponding to the transient fast-mode disturbances or above curve 3 corresponding to the transient slow-mode disturbances for a given value of θ_s. It is seen that acoustic disturbances cannot pass behind the SW for a zero angle of propagation (curve 2) and for all angles of SW incidence observed in the experiments. Thus, interaction of slow acoustic waves with the SW allows only disturbances of the entropy-vortex mode to propagate behind the SW in the range of angles θ_s under consideration. Acoustic waves are expected to decay exponentially behind the SW front.

Figure 8 shows the wave diagrams for the case of interaction of acoustic waves with different angles of incidence onto the SW. The angle θ_s with respect to the flow direction is assumed to be 10°. A Cartesian coordinate system is used, where the SW is directed along the y axis. Figure 8a shows the curves for the slow (curve 3) and fast (curve 1) acoustic waves in an undisturbed hypersonic flow with $M_\infty = 21$. The point of curve 3 corresponds to the zero angle of incidence of the acoustic wave. Figure 8b shows similar curves for the slow and fast acoustic waves (curves 3 and 1) and entropy-vortex disturbances (curve 4) that passed behind the SW. In linear interaction of plane waves with the shock wave, the y component of the wave vector for transient waves remains unchanged. This allows us to find the wave vector of disturbances that passed through the shock wave [2]. It is seen from Fig. 8b that curve 2 ($k_y = \text{const}$) does not cross curves 1 and 3; hence, the condition of existence of acoustic waves behind the shock wave is not satisfied. The wave diagrams for other angles of SW incidence observed in the experiments are similar to those plotted in Fig. 8. At the same time, curves 2 and 4 always intersect each other, and entropy-vortex disturbances arise behind the SW for all angles θ_s.

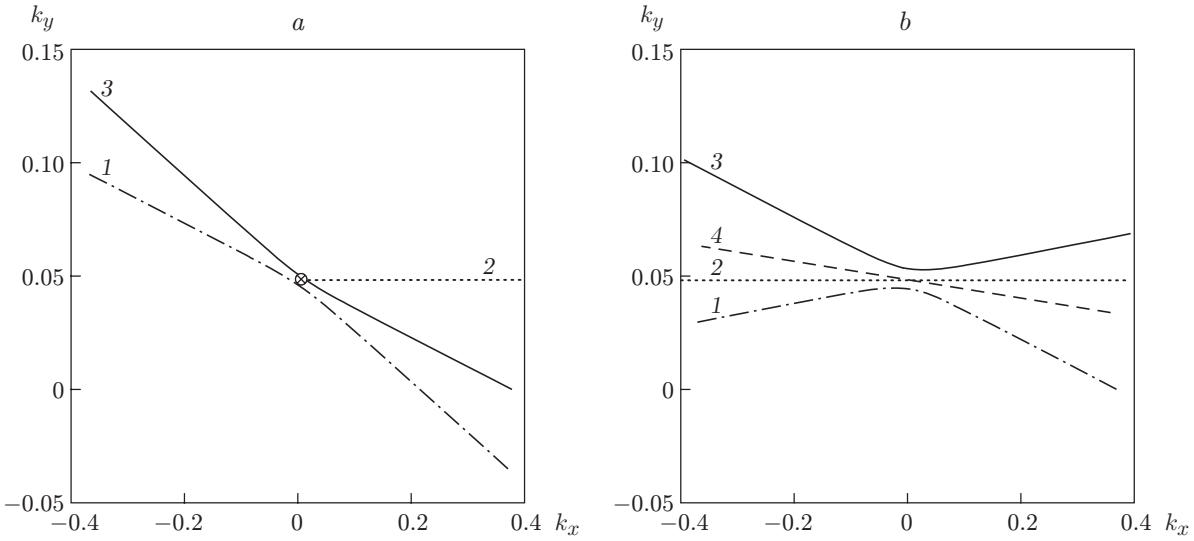

Fig. 8. Wave diagrams ahead of the SW (a) and behind the SW (b): the curves refer to a fast acoustic wave (1), $k_y = \text{const}$ (2), slow acoustic wave (3), and entropy-vortex wave (4).

The wavelengths of vortex disturbances computed by the linear theory of propagation of acoustic waves through the SW are close to the size of vortices obtained by direct numerical simulation (see Fig. 2b).

Thus, the entropy-vortex mode dominates in the region between the shock wave and the boundary-layer edge. The vortex disturbances excite normal-to-surface oscillations of the mean flow in the shock layer, which, in turn, generate density fluctuations observed in the computations and experiments. It should be noted that the prevalence of the entropy-vortex mode at moderate hypersonic Mach numbers is not typical of the boundary layer, where the acoustic mode of instability is mainly developed [3, 4], and can be possibly explained by the mechanism of excitation of disturbances due to SW oscillations, which is typical of this problem.

Conclusions. The values of the Mach number, mean density, and growth rates of density fluctuations are measured in the shock layer on a thermostated flat plate by the Pitot tube and by the method of electron-beam fluorescence.

The field of flow disturbances for the case of interaction of slow external acoustic waves with the shock layer on a flat plate is obtained for the first time for test conditions by means of direct numerical simulation on the basis of the Navier–Stokes equations.

The experimental and computed data on the mean and fluctuating characteristics are in good agreement.

The direct numerical simulation demonstrates the existence of two regions with the maximum density fluctuations: on the SW (with a higher amplitude) and on the boundary-layer edge (with a lower amplitude); the phases of these fluctuations are shifted by 180°. The existence of regions with the maximum density fluctuations is validated by electron-beam measurements. The presence of density fluctuations with similar properties was previously observed in flows of the viscous shock layer type, in particular, in the wake flow and on the compression surface.

It is demonstrated within the framework of the linear theory of interaction of incident acoustic waves with the shock wave that only the entropy-vortex mode is generated owing to interaction of slow external acoustic waves with the bow SW in the viscous shock layer on a flat plate.

A model is proposed to relate density fluctuations in the shock layer, which arise under the action of vortex disturbances, to distributions of the mean density and mean normal velocity.

The authors are grateful to A. A. Maslov for supporting these activities and discussing the results obtained.

This work was supported by the Russian Foundation for Basic Research (Grant Nos. 05-08-33436 and 04-01-00474).

REFERENCES

1. C. L. Chang, M. F. Malik, and M. Y. Hussaini, "Effect of shock on the stability of hypersonic boundary layers," AIAA Paper No. 90-1448 (1990).
2. J. F. McKenzie and K. O. Westphal, "Interaction of linear waves with oblique shock waves," *Phys. Fluids*, **11**, 2350–2362 (1968).
3. K. F. Stetson and R. L. Kimmel, "On hypersonic boundary-layer stability," AIAA Paper No. 92-0737 (1992).
4. H. L. Reed and W. S. Saric, "Linear stability theory applied to boundary layers," *Annu. Rev. Fluid Mech.*, **28**, 389–428 (1996).
5. Y. Ma and X. Zhong, "Receptivity of a supersonic boundary layer over a flat plate. Part 2. Receptivity to freestream sound," *J. Fluid Mech.*, **488**, 79–121 (2003).
6. I. V. Egorov, V. G. Sudakov, and A. V. Fedorov, "Numerical simulation of propagation of disturbances in a supersonic boundary layer," *Izv. Ross. Akad. Nauk, Mekh. Zhidk. Gaza*, No. 6, 33–44 (2004).
7. M. C. Fisher, D. V. Maddalon, L. M. Weinstein, and R. D. Wagner (Jr.), "Boundary-layer Pitot and hot-wire surveys at $M_\infty \approx 20$," *AIAA J.*, **9**, No. 5, 826–834 (1971).
8. J. H. Kemp and F. K. Owen, "Nozzle wall boundary layer at Mach numbers 20 to 47," *AIAA J.*, **10**, No. 7, 872–879 (1972).
9. J. A. Smith and J. F. Driscoll, "The electron-beam fluorescence technique for measurements in hypersonic turbulent flows," *J. Fluid Mech.*, **72**, No. 4, 695–719 (1975).
10. S. J. Cowley and Ph. Hall, "On the instability of hypersonic flow past a wedge," *J. Fluid Mech.*, **214**, 17–42 (1990).
11. N. D. Blackaby, S. J. Cowley, and Ph. Hall, "On the instability of hypersonic flow past a flat plate," *J. Fluid Mech.*, **247**, 369–416 (1993).
12. C. W. Whang and X. Zhong, "Nonlinear interaction of Görtler and second shear modes in hypersonic boundary layers," AIAA Paper No. 2000-0536 (2000).
13. X. Zhong, "Leading-edge receptivity to free-stream disturbances waves for hypersonic flow over a parabola," *J. Fluid Mech.*, **441**, 315–367 (2001).
14. J. Laufer, "Some statistical properties of the pressure field radiated by a turbulent boundary layer," *Phys. Fluids*, **7**, No. 8, 1191–1197 (1964).
15. K. W. Roger, G. B. Wainwright, and K. J. Touryan, "Impact and static pressure measurements in high speed flows with transitional Knudsen numbers," in: *Rarefied Gas Dynamics*, Vol. 2, Academic Press, New York (1966), pp. 151–174.
16. S. G. Mironov and A. A. Maslov, "An experimental study of density waves in hypersonic shock layer on a flat plate," *Phys. Fluids, A*, **12**, No. 6, 1544–1553 (2000).
17. A. Suresh and H. T. Huynh, "Accurate monotonicity-preserving schemes with Runge–Kutta stepping," *J. Comput. Phys.*, **136**, Part 1, 83–99 (1997).
18. A. N. Kudryavtsev and D. V. Khotyanovsky, "Numerical simulation of compressible shear layer development with weighted ENO schemes," in: *Computational Fluid Dynamics*, Proc. of the ECCOMAS Conf. (Athens, Greece, September 7–11, 1998), Vol. 1, Part 2, John Wiley and Sons, Chichester (1998), pp. 900–905.
19. M. N. Kogan, *Rarefied Gas Dynamics* [in Russian], Nauka, Moscow (1974).
20. A. A. Maslov, S. G. Mironov, and V. M. Aniskin, "Hypersonic shear layer stability experiments," *J. Spacecraft Rockets,* **42**, No. 6, 999–1004 (2005).
21. V. M. Aniskin and S. G. Mironov, "Evolution of controlled disturbances in the shock layer on the compression surface," *J. Appl. Mech. Tech. Phys.*, **44**, No. 5, 626–633 (2003).